Journal of Molecular Spectroscopy **201,** 95–108 (2000)
doi:10.1006/jmsp.2000.8070, available online at http://www.idealibrary.com on IDEAL®

Analysis of the "Unusual" Vibrational Components of Triply Degenerate Vibrational Mode ν_6 of $Mo(CO)_6$ Based on the Classical Interpretation of the Effective Rotation–Vibration Hamiltonian

G. Dhont,* D. Sadovskiĭ,* B. Zhilinskiĭ,* and V. Boudon†

*MREID, Université du Littoral, 145 av. M. Schumann, F-59140 Dunkerque, France; and †Laboratoire de Physique de l'Université de Bourgogne, CNRS, B.P. 47870, F-21078 Dijon Cedex, France

E-mail: zhilin@univ-littoral.fr, boudon@jupiter.u-bourgogne.fr

Received September 14, 1999; in revised form January 14, 2000

Rotational structure of the triply degenerate vibrational state $\nu_6(F_{1u})$ of the octahedral molecule $Mo(CO)_6$ is analyzed qualitatively on the basis of classical mechanics. We show that the energy level redistribution between the vibrational components of $\nu_6(F_{1u})$ occurs due to rotational excitation and is related to the formation of singular points of classical rotational energy surfaces. The singularity is stable under small variations of parameters of the effective rovibrational Hamiltonian. Parameters responsible for the persistence of this phenomenon are specified. Comparison with quantum calculations demonstrates the high qualitative and quantitative accuracy of our classical analysis. © 2000 Academic Press

Key Words: rovibrational interactions; spherical top molecules; quantum-classical correspondence.

1. INTRODUCTION

Modern spectroscopic studies produce an increasing amount of information on the rotational structure of different vibrational states of a constantly widening variety of molecules. Typically this information is represented as a list of effective parameters which can be used to reproduce quantum energies, transition frequencies, and intensities with sufficiently high precision. On the other hand, we can use the same effective parameters to describe global qualitative features of the systems of energy levels and corresponding spectral transitions. For example, we can study formation of vibrational bands, energy level clusters, modification of the cluster structure, etc. Such qualitative analysis attracts increasing attention of spectroscopists. It is mainly based on the theory of classical dynamical systems which at the first sight does not seem to be very relevant to "purely" quantum systems such as a simple molecule in a specific quantum vibrational state. At the same time, several classical approaches were used very successfully over the last two decades to interpret quantum effects observed in rotational, vibrational, and electronic structure (see Refs. (*1–19*)). In fact, once the advantages of qualitative classical analysis are appreciated in full, this analysis will become a natural complement of practically every spectroscopic study.

Classical interpretation of molecular spectra was pioneered by Dorney and Watson (*1*), who successfully explained the existence of six- and eightfold degenerate clusters of rotational levels of spherical top molecules in terms of stable classical rotation (precession) around six and eight symmetry axes of the type C_4 and C_3, respectively. This approach was largely advanced in the works by Harter and co-workers (*2, 3, 4, 6*), who introduced the so-called *rotational energy surface* (RES) to describe the structure of quantum rotational multiplet of a nondegenerate isolated vibrational state (*4*). Pavlichenkov and Zhilinskiĭ (*5*) considered and interpreted quantum analogues of classical bifurcations of RESs which occur naturally when rotational excitation (i.e., quantum number J) increases. The RES construction was generalized to a group of quasi-degenerate vibrational levels in (*6, 7*). Crossings of the RESs representing such a group, known also as *diabolic points,* were analyzed in (*8*). General rules governing level redistribution which takes place at such crossings in tetrahedral molecules were formulated in a series of works by Brodersen and Zhilinskiĭ (*14, 15, 16*). Generalizations to other systems, such as vibrational polyads, formulation of the qualitative analysis on the basis of topological and group theoretical arguments, and examples are discussed in (*12, 11, 17*). In this work we present classical qualitative *and* quantitative interpretation of the effective quantum Hamiltonian of the octahedral molecule $Mo(CO)_6$ whose triply degenerate vibrational state ν_6 reconstructed by Asselin *et al.* (*20*) is of a quite unusual rovibrational structure. Reference (*20*) describes the first high-resolution spectroscopic study of this heavy spherical top. The authors where able to fit data from the ν_6 band up to $J = 74$.

2. EFFECTIVE HAMILTONIAN AND QUANTUM-CLASSICAL CORRESPONDENCE

The octahedral molecule $Mo(CO)_6$ possesses 13 normal modes of vibration (*21*). We study the triply degenerate C–O

0022-2852/00 $35.00
Copyright © 2000 by Academic Press
All rights of reproduction in any form reserved.

stretch fundamental state ν_6 of symmetry F_{1u}. This vibrational state can be considered as isolated because (i) among the six C–O stretch fundamentals ($A_{1g} + E_g + F_{1u}$), it is the only state of the u symmetry type; (ii) for the O_h molecules interactions between u and g states are forbidden; and (iii) C–O stretch fundamentals lie in the 2000 cm^{-1} region, well above all other vibrations, of the molecule (stretches Mo–C, bends C–Mo–C, and Mo–C–O, etc.).

2.1. Effective Quantum Rotation–Vibration Hamiltonian

The effective Hamiltonian $\tilde{H}$ for the isolated $v_6 = 1$ vibrational state can be represented as a series of coupled terms $H^{\Omega(K,n\Gamma)}$ constructed from vibrational and rotational tensor operators, $V^{(\Gamma)}$ and $R^{\Omega(K,n\Gamma)}$, respectively,

$$H^{\Omega(K,n\Gamma)} = [V^{(\Gamma)} \otimes R^{\Omega(K,n\Gamma)}]^{(A_{1g})}. \quad [1]$$

Vibrational operators are in turn built as symmetrized tensor products of creation and annihilation operators for mode ν_6, $a_6^{+(F_{1u})}$, and $a_6^{(F_{1u})}$,

$$V_\sigma^\Gamma = [a_6^{+(F_{1u})} \otimes a_6^{(F_{1u})}]_\sigma^{(\Gamma)}, \quad [2]$$

while rotational tensor operators are constructed from elementary angular momentum operators J_x, J_y, and J_z (*22*). Including all possible rovibrational operators up to order three, we obtain the Hamiltonian

$$\begin{aligned}\tilde{H} = {} & k_1 V^{(A_{1g})} + k_2 R^{2(0_g,A_{1g})} + k_3 H^{1(1_g,F_{1g})} \\ & + k_4 H^{2(0_g,A_{1g})} + k_5 H^{2(2_g,E_g)} + k_6 H^{2(2_g,F_{2g})} \\ & + k_7 H^{3(1_g,F_{1g})} + k_8 H^{3(3_g,F_{1g})}.\end{aligned} \quad [3]$$

The first three terms in $\tilde{H}$ describe the degenerated three dimensional harmonic oscillator, the spherical-top rigid rotor, and the Coriolis interaction, respectively. Parameters k_i ($i = 1, \ldots, 8$) are related to those in Ref. (*20*) as shown in Table 1. Parameters k_1, k_2, and k_4 define the scalar contribution to the rotational energy

$$E_s(\mathcal{J}) = \frac{1}{\sqrt{3}} k_1 - \frac{4}{\sqrt{3}} k_2 \mathcal{J}^2 - \frac{4}{3} k_4 \mathcal{J}^2, \quad [4]$$

where

$$\mathcal{J} = \sqrt{J(J+1)} \quad [5]$$

is the amplitude of the angular momentum and J is the rotation quantum number. The term $E_s(\mathcal{J})$ is common to all levels within the rotational multiplet of ν_6. Consequently, parameters k_1, k_2, and k_4 are of no interest to the study of the internal structure of this multiplet. For convenience we will ignore k_2 and plot the so-called "reduced energies" calculated with k_2 set to zero.

TABLE 1
Parameters of the Effective Rovibrational Hamiltonian for the ν_6 Fundamental Band of $Mo(CO)_6$

Parameter			Value (cm^{-1})
This work	Notation of Asselin *et al.* [20]	Notation of Robiette *et al.* [24]	
k_1	$\sqrt{3}t^{0(0,A_{1g})F_{1u}F_{1u}}_{\{6\}\{6\}}$	$\sqrt{3}\nu_6$	3473.60352
k_2	$-\frac{\sqrt{3}}{4}t^{2(0,A_{1g})A_{1g}A_{1g}}_{\{0\}\{0\}}$	$-\frac{\sqrt{3}}{4}B_0$	(Set to 0)
k_3	$-\frac{1}{\sqrt{3}}t^{1(1,F_{1g})F_{1u}F_{1u}}_{\{6\}\{6\}}$	$-\sqrt{6}(B\zeta)_6$	2.10×10^{-4}
k_4	$-\frac{3}{4}t^{2(0,A_{1g})F_{1u}F_{1u}}_{\{6\}\{6\}}$	$-\frac{3}{4}(B_6 - B_0)$	9.6390×10^{-6}
k_5	$\frac{1}{\sqrt{2}}t^{2(2,E_g)F_{1u}F_{1u}}_{\{6\}\{6\}}$	$-\frac{\sqrt{2}}{4}\alpha_{220}$	
		$-3\sqrt{2}\alpha_{224}$	-7.07×10^{-6}
k_6	$\frac{1}{\sqrt{3}}t^{2(2,F_{2g})F_{1u}F_{1u}}_{\{6\}\{6\}}$	$-\frac{\sqrt{3}}{4}\alpha_{220}$	
		$+2\sqrt{3}\alpha_{224}$	7.68×10^{-7}
k_7	$-\frac{1}{\sqrt{3}}t^{3(1,F_{1g})F_{1u}F_{1u}}_{\{6\}\{6\}}$	$\frac{3\sqrt{2}}{8}F_{110}$	8.83×10^{-9}
k_8	$-\frac{1}{\sqrt{3}}t^{3(3,F_{1g})F_{1u}F_{1u}}_{\{6\}\{6\}}$	$-\frac{\sqrt{15}}{2}F_{134}$	-8.03×10^{-9}

Note. Numerical values are taken from Ref. (*20*).

2.2. Classical Symbol and Rotational Energy Surfaces (RES)

We follow Refs. (*3, 6, 7, 10*) where the quantum description of the vibrational part of the Hamiltonian is combined with the classical description of the rotational degrees of freedom. Using the vibrational basis functions

$$\{|v_{6x}, v_{6y}, v_{6z}\rangle\} = \{|1, 0, 0\rangle, |0, 1, 0\rangle, |0, 0, 1\rangle\}, \quad [6]$$

and expanding all tensor notation in [3] we get the following matrix of the Hamiltonian $\tilde{H}$,

$$\tilde{H} = \begin{pmatrix} H_{11} & H_{21}^* & H_{31}^* \\ H_{21} & H_{22} & H_{32}^* \\ H_{31} & H_{32} & H_{33} \end{pmatrix}, \quad [7]$$

Copyright © 2000 by Academic Press

with

$$
\begin{aligned}
H_{11} &= \frac{1}{\sqrt{3}}k_1 - \frac{4}{\sqrt{3}}k_2\mathcal{J}^2 - \frac{4}{3}k_4\mathcal{J}^2 \\
&\quad - \frac{2\sqrt{2}}{3}k_5(2J_x^2 - J_y^2 - J_z^2), \\
H_{22} &= \frac{1}{\sqrt{3}}k_1 - \frac{4}{\sqrt{3}}k_2\mathcal{J}^2 - \frac{4}{3}k_4\mathcal{J}^2 \\
&\quad - \frac{2\sqrt{2}}{3}k_5(2J_y^2 - J_z^2 - J_x^2), \\
H_{33} &= \frac{1}{\sqrt{3}}k_1 - \frac{4}{\sqrt{3}}k_2\mathcal{J}^2 - \frac{4}{3}k_4\mathcal{J}^2 \\
&\quad - \frac{2\sqrt{2}}{3}k_5(2J_z^2 - J_x^2 - J_y^2), \\
H_{21} &= -\frac{2}{\sqrt{3}}k_6(J_xJ_y + J_yJ_x) + \frac{i}{\sqrt{6}}\left(2k_3 - \frac{8}{\sqrt{3}}k_7\mathcal{J}^2\right. \\
&\quad \left. + \frac{4\sqrt{2}}{\sqrt{5}}k_8(2J_z^2 - 3J_x^2 - 3J_y^2 + 1)\right)J_z, \\
H_{31} &= -\frac{2}{\sqrt{3}}k_6(J_xJ_z + J_zJ_x) - \frac{i}{\sqrt{6}}\left(2k_3 - \frac{8}{\sqrt{3}}k_7\mathcal{J}^2\right. \\
&\quad \left. + \frac{4\sqrt{2}}{\sqrt{5}}k_8(2J_y^2 - 3J_z^2 - 3J_x^2 + 1)\right)J_y, \\
H_{32} &= -\frac{2}{\sqrt{3}}k_6(J_yJ_z + J_zJ_y) + \frac{i}{\sqrt{6}}\left(2k_3 - \frac{8}{\sqrt{3}}k_7\mathcal{J}^2\right. \\
&\quad \left. + \frac{4\sqrt{2}}{\sqrt{5}}k_8(2J_x^2 - 3J_y^2 - 3J_z^2 + 1)\right)J_x,
\end{aligned}
\qquad [8]
$$

In these formulae rotational operators J_x, J_y, and J_z are converted to classical dynamical variables

$$(J_x, J_y, J_z) = \mathcal{J}(\sin\theta\cos\phi, \sin\theta\sin\phi, \cos\theta), \qquad [9]$$

where angles ϕ and θ define the axis of rotation and $\mathcal{J}$ is the constant amplitude of the classical angular momentum. The angles (θ, ϕ) are the coordinates on the classical phase space for the rotational motion, called rotational *phase sphere* (*4, 6, 7, 8*). Diagonalization of matrix [7] for a given value of $\mathcal{J}$ and for each direction (θ, ϕ) gives three eigenvalues $E_i^{\mathcal{J}}(\theta, \phi)$ ($i = -1$, 0, and $+1$) which represent three classical rotational energy surfaces defined as functions on the rotational phase sphere.

TABLE 2
Principal Stationary Rotation Axes of an Octahedral Molecule

axis	$[J_x, J_y, J_z]$	(θ, ϕ)	number
C_4	$[0, 0, 1]$	$(0, 0)$	3
C_3	$[1, 1, 1]/\sqrt{3}$	$(\arctan\sqrt{2}, \pi/4)$	4
C_2	$[1, 1, 0]/\sqrt{2}$	$(\pi/2, \pi/4)$	6

Note. Coordinates for the particular axes used in this work and number of equivalent axes of each symmetry type.

2.3. Energy of Rotation around Principal Stationary Axes

We are particularly interested in the values of $E_i^J(\theta, \phi)$ for stationary axes of rotation. Principal stationary axes of any O_h symmetric molecule are its symmetry axes C_4, C_3, and C_2. The O_h group has several equivalent by symmetry axes of each kind and naturally the value of E_i^J for each of the equivalent axes is the same. More precisely, equivalent by symmetry points (θ, ϕ) form an orbit of *equivalent* points on the rotational phase sphere. The principal axes are *always* stationary, and moreover, axes C_4 and C_3 should be stable for any generic Hamiltonian. This means that generically functions E_i^J have a nondegenerate maximum, a minimum, or a saddle at the corresponding points on the phase sphere for any J. These points form *critical orbits* (*23*) with local symmetry C_2, C_3, and C_4. The C_4 and C_3 points can either be a maximum or a minimum, while the C_2 point can also be a saddle. To calculate E_i^J we choose one representative in each critical orbit indicated in Table 2.

Simple analytical expressions can be found for the energies on the critical orbits by diagonalizing the matrix [7]. For C_4 axes we obtain

$$
\begin{aligned}
E_0(\mathcal{J}) &= E_s(\mathcal{J}) - \frac{4\sqrt{2}}{3}k_5\mathcal{J}^2, \\
E_{\pm1}(\mathcal{J}) &= E_s(\mathcal{J}) + \frac{2\sqrt{2}}{3}k_5\mathcal{J}^2 \pm \sqrt{\frac{2}{3}}k_3\mathcal{J} \\
&\quad \mp \frac{4\sqrt{2}}{3}k_7\mathcal{J}^3 \pm \frac{4}{\sqrt{15}}k_8(2\mathcal{J}^3 + \mathcal{J}),
\end{aligned}
\qquad [10]
$$

where E_s is the scalar contribution [4]. The three eigenvalues for C_3 axes are

$$
\begin{aligned}
E_0(\mathcal{J}) &= E_s(\mathcal{J}) - \frac{8\sqrt{3}}{9}k_6\mathcal{J}^2, \\
E_{\pm1}(\mathcal{J}) &= E_s(\mathcal{J}) + \frac{4\sqrt{3}}{9}k_6\mathcal{J}^2 \pm \sqrt{\frac{2}{3}}k_3\mathcal{J} \\
&\quad \mp \frac{4\sqrt{2}}{3}k_7\mathcal{J}^3 \mp \frac{4}{\sqrt{15}}k_8\left(\frac{4}{3}\mathcal{J}^3 - \mathcal{J}\right).
\end{aligned}
\qquad [11]
$$

Copyright © 2000 by Academic Press

The three eigenvalues for C_2 axes are

$$E_0(\mathcal{J}) = E_s(\mathcal{J}) - \frac{\sqrt{2}}{3} k_5 \mathcal{J}^2 - \frac{2}{\sqrt{3}} k_6 \mathcal{J}^2,$$

$$E_{\pm 1}(\mathcal{J}) = E_s(\mathcal{J}) + \frac{\sqrt{2}}{6} k_5 \mathcal{J}^2 + \frac{1}{\sqrt{3}} k_6 \mathcal{J}^2 \pm \frac{1}{6} \mathcal{J} \sqrt{3a^2 \mathcal{J}^2 + 6b^2}, \quad [12]$$

with

$$a = 2k_6 - \sqrt{6}\, k_5,$$

$$b = 2k_3 - \frac{8}{\sqrt{3}} k_7 \mathcal{J}^2 + \sqrt{\frac{2}{5}} k_8 (4 - 2\mathcal{J}^2). \quad [13]$$

It should be pointed out that the rotational structure of a triply degenerate state of a spherical top molecule has been studied numerically by Harter and co-workers (*3*) using a simpler model. Equations [10], [11], and [12] give an analytical classical description for a more elaborated effective Hamiltonian [3].

2.4. Quantum-Classical Correspondence

Figure 1 gives a general idea of the correspondence between our formulae for the classical stationary rotation energies $E_i(\mathcal{J})$ and the structure of quantum multiplet obtained in (*20*). Contrary to the quantum spectrum which appears quite complicated due to a great number of individual levels, the classical RES "spectrum" is strikingly simple. Yet this simple classical description retains all essential qualitative information on the system of quantum levels in a very concise and efficient way. To understand more how it works notice first that the splitting of the multiplet is well delimited by an absolute maximum and minimum $E_i(\mathcal{J})$ at each given J, then identify three groups of quantum levels which form three diverging "branches" as the value J increases and remark how well the three groups of classical values $E_i^{C_4}(\mathcal{J})$, $E_i^{C_2}(\mathcal{J})$, and $E_i^{C_3}(\mathcal{J})$ represent branches $i = 0$ and ± 1. As first shown in (*1*), each sufficiently stable equilibrium $E_i(\mathcal{J})$ corresponds to a regular sequence of quasi-degenerated groups of quantum levels called *clusters.* The number of levels in each cluster equals the number of equivalent stationary points of RES which in turn equals twice (to account for two directions of classical rotation) the number of equivalent axes. Thus for $J > 15$ we observe a particularly prominent series of sixfold clusters in the upper part of the ν_6 multiplet. These clusters correspond to stable rotation around C_4 axes.

2.4.1. Regular cluster sequences. Cluster sequences can be well reproduced using an oscillator approximation near each stable stationary point of RES. If the frequency of the oscillator is sufficiently large in comparison to the rotational quantum $B\mathcal{J}$ then the corresponding quantum spectrum has a regular sequence of levels with different projection of the angular momentum on the particular stationary axis, $m = J, J - 1, \ldots$. To find the harmonic part (the frequency) of the oscillator potential and to estimate the stability of the stationary point (*10*) of RES, we calculate the value of Hessian:

$$h_i^J(\theta, \phi) = \left(\frac{\partial^2 E_i^J}{\partial \theta^2}\right)\left(\frac{\partial^2 E_i^J}{\partial \phi^2}\right) - \left(\frac{\partial^2 E_i^J}{\partial \theta \partial \phi}\right)^2. \quad [14]$$

Positive and negative values of h_i^J correspond to stable and unstable classical rotation, respectively. A zero Hessian $h_i^J = 0$ for some critical value J_c indicates a bifurcation in the limiting classical problem and a modification of the rotational cluster structure.

2.4.2. Branches of levels. "Typical" rotational multiplets of triply degenerate fundamentals of spherical top molecules consist of three branches (*25*) also called *vibrational components.* The branches are formed due to the Coriolis interaction term which is

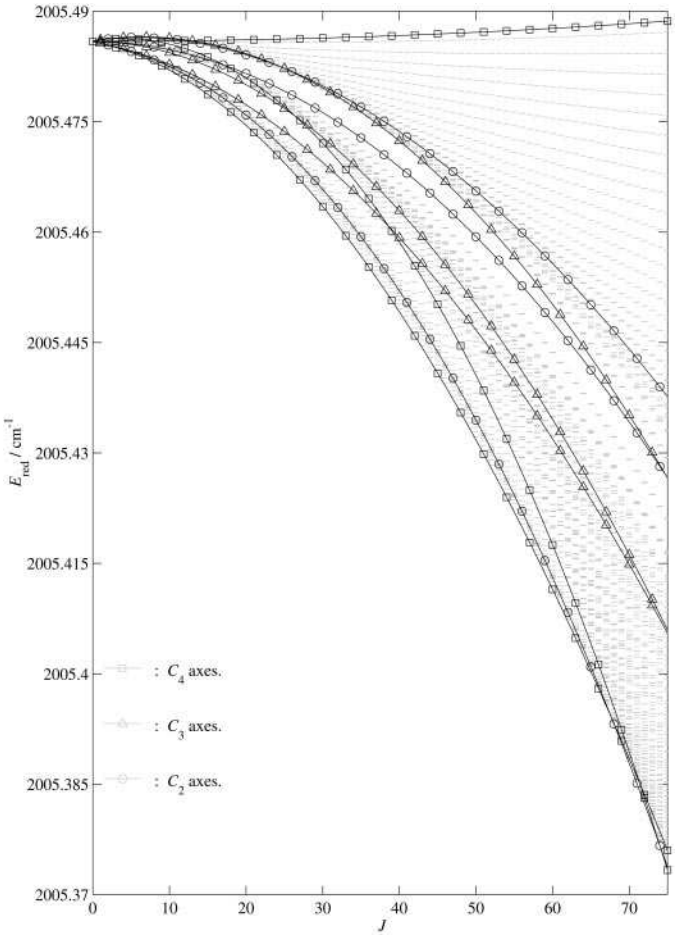

FIG. 1. Quantum (gray horizontal bars) and semiclassical energies $E_i(J)$ with $i = 0, \pm 1$ (solid lines) in the interval $0 \leq J \leq 75$.

Copyright © 2000 by Academic Press

typically dominant, at least when the values of J are sufficiently low. When J increases, such branches diverge linearly. At each given J the number of levels $2R + 1$ in each branch is defined by the quantum number $R = J - 1$, J, and $J + 1$ and hence the branches are labeled by $i = -1, 0, 1$. The structure is, of course, a textbook example of angular momentum coupling: the angular momentum $\mathbf{R}$ is a sum of $\mathbf{J}$ and the angular momentum $\mathbf{l} = 1$ of the triply degenerate vibrational mode, the corresponding coupling term $\mathbf{l} \cdot \mathbf{J}$ describes Coriolis interaction.

As has already been noted in (*20*), the first-order Coriolis interaction constant k_3 of the ν_6 state is so small (see Table 1) that at $J \approx 10$ the contribution of the second-order terms with constants k_5 and k_6 surpasses that of the Coriolis term. This results in a very different branch structure which is formed at higher values of J. Classical energies reproduce this transition qualitatively correctly. Many interesting phenomena can be seen and are analyzed in the next sections.

The main phenomenon which corresponds in the classical limit to the change of the branch structure of the quantum spectrum is the formation of the degeneracy points (singularities or diabolic points) of RESs (*7, 8*). Typically two RESs become degenerated at some isolated value J_{crit} and depending on the nature of singularity, the Hessian function $h_i(J)$ has a particular discontinuity. When this happens the RESs are no longer isolated and we should consider the connected surfaces as one multivalued function. Formation of an isolated degeneracy point of RESs is reflected in the quantum energy spectrum as a redistribution of energy levels between branches, or in other words as a reorganization of vibrational components (*8*).

In Section 3 we characterize briefly possible changes of the branch structure of the rotational multiplet $v_6^{F_{1u}} = 1$ of an octahedral molecule on the basis of the theory for tetrahedral molecules developed in (*14, 15, 16*). In Section 4 we return to the analysis of the concrete situation in $Mo(CO)_6$.

3. VIBRATIONAL COMPONENTS OF OCTAHEDRAL MOLECULES

Rotational structure of degenerated vibrational states of spherical top molecules exhibits distinct rotational multiplets for each vibrational component (branch). These multiplets are particularly visible at sufficiently low rotational excitation.

Analysis of possible decompositions of all rotational states into several distinct components begins with the observation that all rotational levels of the vibrational state $\nu_6(F_{1u})$ at a given J form a reducible representation of the O_h group which can be written symbolically as

$$\Gamma_{\text{rv}} = F_{1u} \times \mathcal{D}^{(J_g)}, \qquad [15]$$

where $\mathcal{D}^{(J_g)}$ stands for the decomposition of the irreducible representation (J_g) of the $O(3)$ group with respect to the O_h group. When all these rovibrational levels decompose into three rotational branches, the reducible representation Γ_{rv} should be represented as a sum of three contributions,

$$\Gamma_{\text{rv}} = \sum_{i=1}^{3} \Gamma_i \times \mathcal{D}^{((J+\Delta_i)_g)}, \qquad [16]$$

where Δ_i and Γ_i are independent on J and $\mathcal{D}^{((J+\Delta_i)_g)}$ denotes a reducible representation of the $O(3)$ group with the effective weight $J + \Delta_i$. Naturally $\Delta_1 + \Delta_2 + \Delta_3 = 0$. Each number Δ_i defines an effective rotational quantum number of the corresponding vibrational component (branch) i and therefore the number of rotational states in this component.

The one-dimensional representations of the O_h group Γ_1, Γ_2, and Γ_3 which enter in [16] are effective symmetries of the corresponding vibrational components $i = 1, 2, 3$. The O_h group has four one-dimensional representations and the corresponding four possible types of vibrational components are

$$A_{1g} \times \mathcal{D}^{((J+\Delta)_g)} \equiv \mathcal{D}_{1g}^{(J+\Delta)}, \qquad [17]$$

$$A_{1u} \times \mathcal{D}^{((J+\Delta)_g)} \equiv \mathcal{D}_{1u}^{(J+\Delta)}, \qquad [18]$$

$$A_{2g} \times \mathcal{D}^{((J+\Delta)_g)} \equiv \mathcal{D}_{2g}^{(J+\Delta)}, \qquad [19]$$

$$A_{2u} \times \mathcal{D}^{((J+\Delta)_g)} \equiv \mathcal{D}_{2u}^{(J+\Delta)}. \qquad [20]$$

(Above we introduce full and shortened notation.)

In our case the symmetry of the vibrational state ν_6 is F_{1u} and consequently all Γ_i should be of type u, i.e., either A_{1u} or A_{2u}. The well-known first-order Coriolis splitting of the F_{1u} vibrational state into three components with effective quantum numbers $R = J + 1$, J, and $J - 1$ corresponds to a particular form of the decomposition [16]

$$F_{1u} \times \mathcal{D}^{(J_g)} = \sum_{\delta=0,\pm1} A_{1u} \times \mathcal{D}^{((J+\delta)_g)} \qquad [21]$$

$$= \mathcal{D}_{1u}^{(J+1)} + \mathcal{D}_{1u}^{(J)} + \mathcal{D}_{1u}^{(J-1)} \qquad [22]$$

(represented both in full and short notation).

By means of a formal group-theoretical analysis similar to that in (*14*) we can find all possible decompositions of the rotational multiplet [15] into three vibrational components. Below are some examples of such alternative decompositions:

$$F_{1u} \times \mathcal{D}^{(J_g)} = \mathcal{D}_{1u}^{(J\pm1)} + \mathcal{D}_{2u}^{(J\mp3)} + \mathcal{D}_{2u}^{(J\pm2)}, \qquad [23]$$

$$F_{1u} \times \mathcal{D}^{(J_g)} = \mathcal{D}_{2u}^{(J\pm1)} + \mathcal{D}_{1u}^{(J\mp3)} + \mathcal{D}_{2u}^{(J\pm2)}. \qquad [24]$$

When we describe possible decompositions into individual vibrational components, we should also consider what elementary modifications of the band structure can occur when rota-

Copyright © 2000 by Academic Press

tional excitation increases, i.e., when the value of J, the only parameter, is varied.

In the next section we will observe one of the unusual decompositions [23] in the structure of rovibrational energy levels reconstructed from the experimental data for the ν_6 band of $Mo(CO)_6$. At low values of J we will also observe the familiar structure [22] and analyze how this structure is rearranged when J increases.

4. QUALITATIVE ANALYSIS OF THE ROTATIONAL STRUCTURE OF THE $\nu_6 = 1$ STATE OF $Mo(CO)_6$

Qualitative analysis of the rotational structure of a degenerate vibrational state has two steps. First we describe individual vibrational components (branches) and study their eventual modifications occurring when rotational excitation increases. Next we consider the rotational cluster structure of each individual vibrational component and its possible modifications.

As we already noted in Section 2.4.2 above, the first-order Coriolis interaction constant k_3 of the $\nu_6 = 1$ state of $Mo(CO)_6$ is so small that the three Coriolis components originally formed at low J interact strongly and $R = J - 1, J, J + 1$ is no longer a good quantum number when J increases. The structure of the three components changes when $J \approx 8$.

4.1. The $0 \leq J \leq 25$ Region

To understand the situation let us first focus on the low J region shown in Fig. 2. For $J < 8$, we can see the three Coriolis components containing $2J - 1$, $2J + 1$, and $2J + 3$ levels, respectively. The corresponding decomposition [22] can be confirmed by comparing the symmetries of the calculated quantum states to the decomposition $\mathcal{D}^{(R)}$ of the weight-R irreducible representation of the rotation group $O(3)$ into irreducible representations of O_h multiplied by the appropriate factor $\Gamma_i = A_{1u}$ defined in [21]. As an example consider the rotational multiplet for $J = 5$

$$
J = 5 \left\{ \begin{array}{ll}
R = J - 1 = 4 & \left\{ \begin{array}{ll} A_1 & 2005.486454 \\ F_1 & 2005.486473 \\ E & 2005.486485 \\ F_2 & 2005.486510 \end{array} \right. \\
R = J = 5 & \left\{ \begin{array}{ll} F_1 & 2005.485724 \\ E & 2005.485746 \\ F_2 & 2005.485935 \\ F_1 & 2005.485974 \end{array} \right. \\
R = J + 1 = 6 & \left\{ \begin{array}{ll} E & 2005.484519 \\ F_2 & 2005.484530 \\ A_2 & 2005.484570 \\ F_2 & 2005.484672 \\ F_1 & 2005.484710 \\ A_1 & 2005.484746 \end{array} \right.
\end{array} \right. .
$$

(Parity is always u and has been omitted, wavenumbers are in reciprocal centimeters, degeneracy of levels A, E, and F is 1, 2, and 3.)

When the value of J increases above $J \approx 8$ we can see in Fig. 2 that a number of levels leave the middle branch (formerly $R = J$) and join the upper branch. The three branches persist at the values $J > 8$ but the number of levels in each branch is different. To reproduce this decomposition in terms of an auxiliary quantum number R such that the number of levels in each branch equals $2R + 1$, we should define $R = J + 1$, $J - 3$, and $J + 2$. As an example consider the multiplet for $J = 10$

$$
J = 10 \left\{ \begin{array}{ll}
R = J + 2 = 12\ (\times A_{2u}) & \left\{ \begin{array}{ll} A_2 & 2005.485843 \\ F_2 & 2005.485850 \\ E & 2005.485854 \\ F_1 & 2005.486106 \\ F_2 & 2005.486130 \\ E & 2005.486191 \\ F_1 & 2005.486202 \\ A_1 & 2005.486277 \\ F_1 & 2005.486285 \\ F_2 & 2005.486291 \\ A_2 & 2005.486296 \end{array} \right. \\
R = J - 3 = 7\ (\times A_{2u}) & \left\{ \begin{array}{ll} F_2 & 2005.484712 \\ E & 2005.484761 \\ F_1 & 2005.484798 \\ A_1 & 2005.484876 \\ F_1 & 2005.485019 \\ F_2 & 2005.485048 \end{array} \right. \\
R = J + 1 = 11\ (\times A_{1u}) & \left\{ \begin{array}{ll} F_1 & 2005.482186 \\ F_2 & 2005.482192 \\ A_2 & 2005.482409 \\ F_2 & 2005.482444 \\ E & 2005.482468 \\ F_1 & 2005.482583 \\ F_2 & 2005.482778 \\ E & 2005.482822 \\ F_1 & 2005.482847 \end{array} \right.
\end{array} \right. .
$$

(The parity index u common to all levels is omitted; wavenumbers are in reciprocal centimeters.) To confirm that the new decomposition is of the type [23], we multiply the standard irreducible representations $\mathcal{D}^{(J+2)}$ (upper component) and $\mathcal{D}^{(J-3)}$ (central component) of the $O(3)$ group by A_{2u} to get the true rovibrational symmetries with respect to the O_h group.

It follows that we should use different good quantum numbers for the values of J below and above $J \approx 8$. The modification of the good quantum numbers proceeds as follows:

Copyright © 2000 by Academic Press

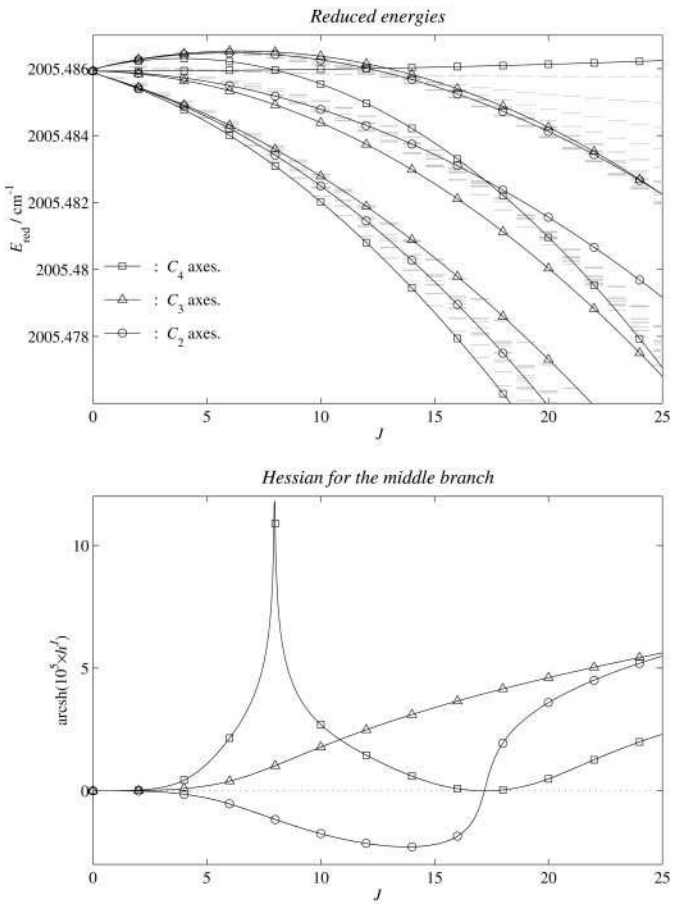

FIG. 2. Above: quantum and classical energies in the interval $0 \leq J \leq 25$ shown by gray horizontal bars and solid curves, respectively. Below: Hessian values h^J for the middle branch $E_0(J)$ at points C_2, C_3, and C_4 shown as $\text{arcsh}(10^5 \times h^J(\theta, \phi))$ in order to increase the range of the plot.

$$\mathcal{D}_{1u}^{(J-1)} \rightarrow \mathcal{D}_{2u}^{(J+2)} : 2(J-1)+1 \overset{+6}{\longrightarrow} 2(J+2)+1,$$

$$\mathcal{D}_{1u}^{(J)} \rightarrow \mathcal{D}_{2u}^{(J-3)} : 2J+1 \overset{-6}{\longrightarrow} 2(J-3)+1,$$

$$\mathcal{D}_{1u}^{(J+1)} \rightarrow \mathcal{D}_{1u}^{(J+1)}.$$

Only the two upper components are involved. The upper component gains six levels while the central component loses six levels. This exchange of six levels can be symbolically represented as a "transition" between the symmetry labels of vibrational components

$$\mathcal{D}_{1u}^{(J)} + \mathcal{D}_{1u}^{(J-1)} \overset{J \approx 8}{\longrightarrow} \mathcal{D}_{2u}^{(J-3)} + \mathcal{D}_{2u}^{(J+2)}. \qquad [25]$$

Note that as in the case of the T_d symmetry (*14*), the label $\mathcal{D}_{1u}^{(K)} \equiv A_{1u} \times \mathcal{D}^{(K_g)}$ can be rewritten as $\mathcal{D}^{(K_u)}$. However, the representation $\mathcal{D}_{2u}^{(K)} \equiv A_{2u} \times \mathcal{D}^{(K_g)}$ cannot be replaced by another representations of the $O(3)$ group with the identical decomposition into irreducible representations of O_h. That is why the specific double index notation for vibrational components should be used in [25] and elsewhere.

Modification of the labeling scheme for the two upper components (branches) is a result of rotation–vibrational coupling. When the labeling of the components changes at $J \approx 8$, the two classical rotational energy surfaces representing upper and central components of the ν_6 (solid lines in Fig. 2, top) form a *conical intersection point,* also called a diabolic point, in the direction (θ, ϕ) corresponding to the C_4 axes. At the same time the Hessian value goes to infinity (Fig. 2, bottom). The formation of the conical intersection of the two upper RES is illustrated in Fig. 3. There are six conical points formed simultaneously at six equivalent C_4-symmetric points on the phase sphere (two points for each C_4 axis). Since, as suggested in (*8*), each conical point corresponds to the redistribution of one energy level, there are six levels, i.e., a sixfold cluster, transferred between the two components.

Figure 4 summarizes how the RESs change when the value of J increases from $J = 2$ to $J = 11$. These sufficiently low J values can give the impression that the application of classical analysis may not be adequate for the description of quantum energy level system. At the same time the numerical comparison between classical and exact quantum results for the

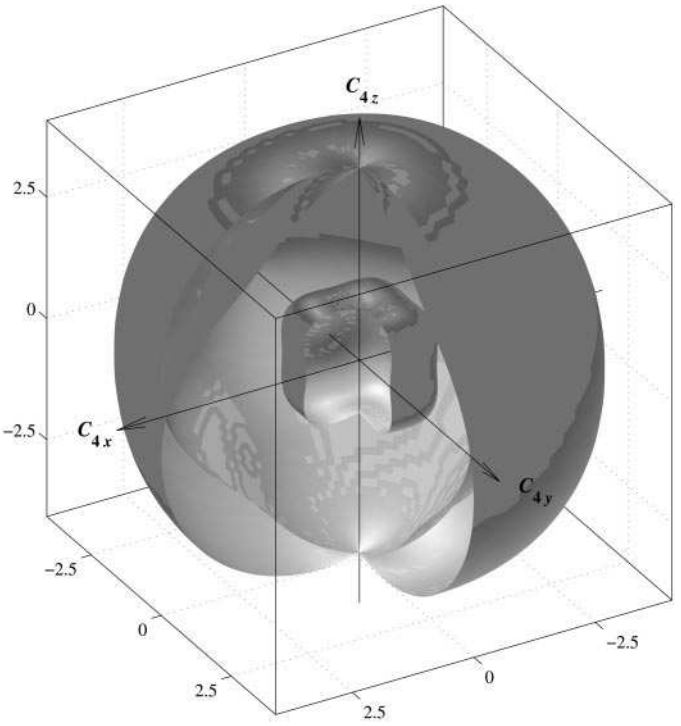

FIG. 3. Rovibrational energy surfaces $E_i^J(\theta, \phi) - E_s$ with $i = 1, 2, 3$, $J = 8$, and $E_s = 2005.482$ cm^{-1}. Coordinates are chosen along the three C_4 symmetry axes (arrows) and are labeled in 10^{-3} cm^{-1}.

Copyright © 2000 by Academic Press

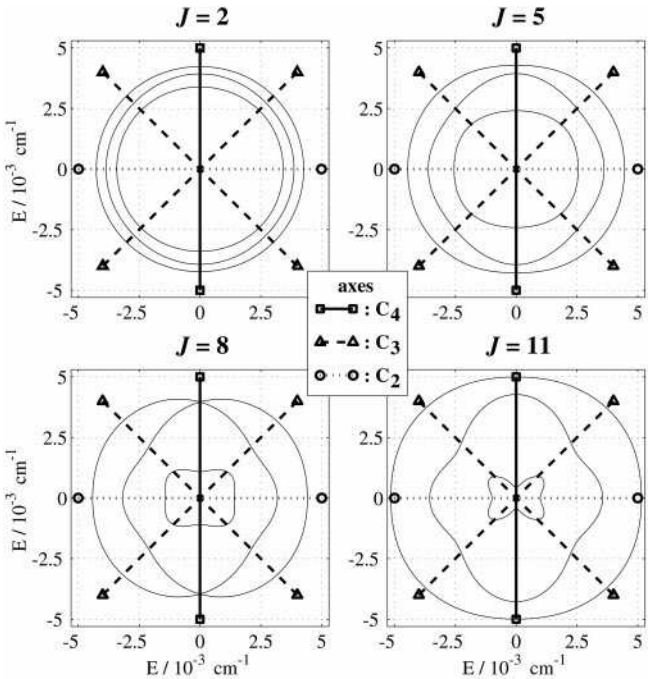

FIG. 4. Cuts of the rotational energy surfaces in the plane $\phi = \pi/4$ for different values of J; we took $E_s = 2005.482\ \text{cm}^{-1}$ (see Fig. 3), except in the case $J = 11$ where we took $E_s = 2005.481\ \text{cm}^{-1}$ for the internal surface.

corresponding Hamiltonian demonstrates the reliability of purely classical analysis. The fact that the rearrangement of branches is a purely topological phenomenon in classical limit ensures its stability under perturbation for quantum Hamiltonian as well. This means that even inclusion of higher order tensorial coupling terms into the Hamiltonian cannot modify the redistribution phenomenon without the appearance of new degeneracy points which in principle can be moved from high J region due to strong perturbation. Such a possibility is not quite realistic because of precise experimental information about rotational structure in the $J = 0$–74 region. Before and after the conical intersection at $J = 8$ we can clearly see three distinct RESs which correspond to three components (branches) of the $\nu_6 = 1$ state. After $J \approx 8$ the decomposition of the rotational multiplet and the labeling scheme remain unchanged up to $J \approx 60$. Our effective rovibrational Hamiltonian is truncated at the third order and is, naturally, less reliable at higher values of J. To the extent this Hamiltonian allows extrapolation we can suggest as to what changes in the structure of the three components may occur. This somewhat formal mathematical analysis is briefly discussed in Section 6.

4.2. *Cluster Structure of the Three Branches*

Once the decomposition of the rotational energy levels into three components (branches) is described, and the redistribution of levels between components occurring near $J = 8$ is understood in terms of connecting RESs, we can further study the cluster structure in each individual component using the corresponding RES. Near maximum and minimum energy of each component we can observe well-pronounced rotational clusters of different kinds which correspond most precisely to the classical rotation around stable stationary axes C_3, C_4, and in some cases C_2. Information on these extremum clusters is presented in Table 3.

The cluster structure in Table 3 corresponds very closely to the classical RES extrema shown by solid lines in Figs. 1 and 2. For example, at the highest and the lowest energy of the lowest component $\mathcal{D}_{1u}^{(J+1)}$ we find eightfold and sixfold degenerate clusters, respectively; they correspond to eight maxima and six minima on the RES in the direction of the C_3 and C_4 symmetry axes.

When $J \simeq 25$, the upper component $\mathcal{D}_{2u}^{(J+2)}$ has 12-fold degenerate clusters at its low energy end and the corresponding RES has a "shallow" global minimum at the 12 points with local symmetry C_2 (Fig. 2). The same component has regular sequences of well-pronounced sixfold clusters starting down from the maximum energy. The corresponding RES maximum is very "deep." In fact the depth of this maximum can be estimated from the large gap between the energy of classical rotation around the C_4 axes and that of rotation around other stationary axes (distance between the corresponding solid lines in Fig. 2). Of course, the quantitative characteristics of the high stability of the rotation around C_4 (and the large depth of the maximum on the RES) is given by the large positive Hessian value at the C_4 point which also gives the frequency of the

TABLE 3
Rotational Clusters with Maximum and Minimum Energy in Each of the Three Components (Branches) of the $\nu_6 = 1$ State of $Mo(CO)_6$ at Different Values of J

component	$J \leq 8$	$J \simeq 12$	$J \simeq 25$	$25 < J \leq 40$
upper	$\mathcal{D}_{1u}^{(J-1)}$ $\begin{cases}\max & 8(C_3)\\ \min & 6(C_4)\end{cases}$	$\mathcal{D}_{2u}^{(J+2)}$ $\begin{cases}\max & 8(C_3)\\ \min & 6(C_4)\end{cases}$	$\mathcal{D}_{2u}^{(J+2)}$ $\begin{cases}\max & 6(C_4)\\ \min & 12(C_2)\end{cases}$	$\mathcal{D}_{2u}^{(J+2)}$ $\begin{cases}\max & 6(C_4)\\ \min & 8(C_3)\end{cases}$
middle	$\mathcal{D}_{1u}^{(J)}$ $\begin{cases}\max & 6(C_4)\\ \min & 8(C_3)\end{cases}$	$\mathcal{D}_{2u}^{(J-3)}$ $\begin{cases}\max & 6(C_4)\\ \min & 8(C_3)\end{cases}$	$\mathcal{D}_{2u}^{(J-3)}$ $\begin{cases}\max & 12(C_2)\\ \min & 6(C_4)\end{cases}$	$\mathcal{D}_{2u}^{(J-3)}$ $\begin{cases}\max & 12(C_2)\\ \min & 6(C_4)\end{cases}$
lower	$\mathcal{D}_{1u}^{(J+1)}$ $\begin{cases}8(C_3)\\ 6(C_4)\end{cases}$	$\mathcal{D}_{1u}^{(J+1)}$ $\begin{cases}8(C_3)\\ 6(C_4)\end{cases}$	$\mathcal{D}_{1u}^{(J+1)}$ $\begin{cases}8(C_3)\\ 6(C_4)\end{cases}$	$\mathcal{D}_{1u}^{(J+1)}$ $\begin{cases}8(C_3)\\ 6(C_4)\end{cases}$

Note. In each case we indicate the symmetry label of the component, the degeneracy of the clusters, and the type of the corresponding stable rotation axes.

Copyright © 2000 by Academic Press

harmonic oscillator approximation for the regular sequence of the C_4 clusters.

A detailed description of elementary modifications of the cluster structure of each component can be given in terms of bifurcations of corresponding RESs (*5, 26*). The method has been well developed in the earlier study of different rotation–vibration multiplets of spherical top molecules (*7, 10, 11, 15*) and practically all bifurcations we observe in this work have already been described before. Thus two bifurcations of the RES corresponding to the central component happen quickly in what appears an "organized" sequence (*7, 27*) when the value of J changes from $J = 16$ to $J = 19$. The moment of each bifurcation can be determined precisely as the moment when the corresponding value of Hessian h^J becomes zero (Fig. 2, bottom). After these bifurcations, rotation around the C_2 axis becomes stable, the C_2 points on the RES become global maxima which are deep enough for the distinct 12-fold clusters to form at $J \approx 25$.

4.3. The $J > 25$ Region

As we can see in Fig. 1, the situation becomes more complicated at higher values of J. At the values of $25 < J \leq 40$, we observe three distinct components (branches) described by $R = J + 1$, $J - 3$, $J + 2$, respectively. Rotational clusters at maximum and minimum energies of each branch are given in Table 3.

The structure of the upper component $\mathcal{D}_{2u}^{(J+2)}$ remains unchanged up to $J \approx 75$ (see Table 3). After $J = 25$ the C_3 minimum on the corresponding RES becomes lower than the C_2 minimum, and the corresponding eightfold clusters can be seen formed at the lower energy end of this component. A large number of sixfold clusters already mentioned above can be well seen at top energies. The corresponding C_4 maximum becomes very deep.

At first sight the structure of the two lower components is more complicated. Starting with $J \approx 40$ the two multiplets begin to overlap in energy (see Fig. 1). For $J > 40$ the C_4 minimum of the $\mathcal{D}_{2u}^{(J-3)}$ (central) RES becomes lower than the C_3 maximum of the $\mathcal{D}_{1u}^{(J+1)}$ (lowest) RES. This, however, does not lead to any qualitative changes in the structure of the two components because the two RES do *not* connect and remain distinct all the way until (at least) $J \approx 70$. Mixing of the wavefunctions localized near the respective C_4 minima of $\mathcal{D}_{2u}^{(J-3)}$ and C_3 maxima of $\mathcal{D}_{1u}^{(J+1)}$ is only possible due to tunneling and is small. The cluster structure of the two components is indicated in Table 3.

5. QUANTUM-CLASSICAL CORRESPONDENCE AND THE DIRECTION OF REDISTRIBUTION

Comparison of classical energies of stationary points (critical orbits) on the two RESs near the conical intersection (diabolic point) and the corresponding part of the quantum energy level spectrum (Fig. 2, top) clearly shows that the levels which transfer between the two components (branches) follow the classical energy at one of the critical points on the RESs involved in the intersection. On the other hand, the classical analysis of the corresponding RESs does not indicate any preference as to which critical point the quantum level should "follow."

In our particular case the two RESs connect at the six C_4 points when $J \approx 8$ and a sixfold cluster is transferred from the central to the upper component (see Fig. 2). We can easily verify that the only terms of the effective Hamiltonian [3] that are essential to the existence of the conical intersection at the C_4 point are the Coriolis term $H^{1(1_g,F_{1g})}$ and the second-order term $H^{2(2_g,E_g)}$ (in the notation of Section 2.1). While a sufficiently large variation of the two respective constants k_3 and k_5 can eliminate the intersection, contributions from other terms in [3] can only modify the energy of the conical point or the value of J at which the intersection occurs. Consequently, a simple model Hamiltonian

$$k_3 H^{1(1_g,F_{1g})} + k_5 H^{2(2_g,E_g)} \qquad [26]$$

can be used to study all qualitative aspects of the energy level redistribution phenomenon in question. If in this model Hamiltonian we set the values of k_3 and k_5 to those in Table 1, the two energies of classical rotation around the C_4 axis (C_4 points on the two RESs) coincide when

$$\sqrt{J(J+1)} = \frac{1}{\sqrt{12}} \left| \frac{k_3}{k_5} \right| \Rightarrow J_{\text{sing}} \approx 8.09, \qquad [27]$$

which is very close to the real value $J \approx 7.97$ for the complete Hamiltonian [3].

In Fig. 5 we compare the quantum energy level spectrum of the model Hamiltonian [26] to the corresponding energy of classical rotation around the C_4 axis. The real situation is reproduced when the Coriolis constant $k_3 > 0$ and $k_5 < 0$ (Fig. 5, top). It can be clearly seen in this figure that classical C_4 curves are in a sense symmetrical with respect to the value J_{sing} at which they cross. On the other hand, quantum energy level pattern breaks this symmetry. Furthermore, a simple change of the sign of the Coriolis term constant $k_3 \rightarrow -k_3$ in [26] does not modify the classical energies. At the same time, changing signs of k_3 flips the quantum energy pattern (Fig. 5, bottom) so that the energy level transfer occurs in the opposite direction when J increases. Of course, changing the sign also modifies the number of quantum levels in each component and thus affects their internal structure.

We now analyze Fig. 5 in more detail. When $J < 8$ we find the familiar structure formed due to the first-order Coriolis interaction. If $k_3 > 0$ the upper, central, and lower branches are labeled by the quantum number $R = J - 1$, J, and $J + 1$, respectively. This order is reversed when $k_3 < 0$. In the former

Copyright © 2000 by Academic Press

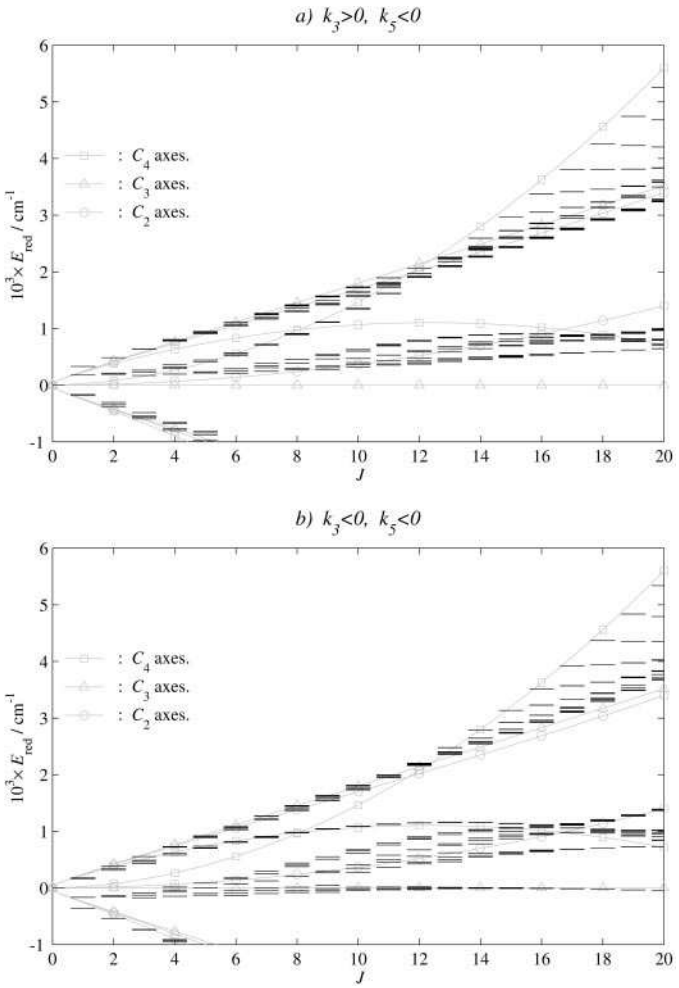

FIG. 5. Quantum (solid horizontal bars) and classical (gray curves) energies for the simple two-parameter model [26] which exhibits different level redistribution for $k_3 > 0$ (top) and $k_3 < 0$ (bottom).

case ($k_3 > 0$, Fig. 5, top), the sixfold cluster moves from the $R = J$ branch to the $R = J - 1$ branch when the value of J increases and passes $J_{sing} = 8$. In other words,

$$\mathcal{D}_{1u}^{(J-1)} \rightarrow \mathcal{D}_{2u}^{(J+2)},$$
$$\mathcal{D}_{1u}^{(J)} \rightarrow \mathcal{D}_{2u}^{(J-3)}, \quad k_3 > 0. \qquad [28]$$

Alternatively ($k_3 < 0$, Fig. 5, bottom), this cluster moves down from the upper branch with $R = J + 1$ to the central branch with $R = J$,

$$\mathcal{D}_{1u}^{(J+1)} \rightarrow \mathcal{D}_{2u}^{(J-2)},$$
$$\mathcal{D}_{1u}^{(J)} \rightarrow \mathcal{D}_{2u}^{(J-3)}, \quad k_3 < 0. \qquad [28]$$

In both cases the sixfold cluster leaves the component with a larger number of levels and joins the "less crowded" component with initially fewer levels. Furthermore, we can show that redistribution in the opposite direction

$$[\mathcal{D}_{1u}^{(J-1)}, \mathcal{D}_{1u}^{(J)}] \overset{?}{\rightarrow} [\mathcal{D}_{\alpha u}^{(J-4)}, \mathcal{D}_{\beta u}^{(J+3)}], \quad k_3 > 0, \qquad [30]$$

$$[\mathcal{D}_{1u}^{(J+1)}, \mathcal{D}_{1u}^{(J)}] \overset{?}{\rightarrow} [\mathcal{D}_{\alpha u}^{(J+4)}, \mathcal{D}_{\beta u}^{(J-3)}], \quad k_3 < 0, \qquad [31]$$

where α and β take the values 1 or 2, is strictly forbidden. Thus in the case of [30] the decomposition of

$$\mathcal{D}_{\alpha u}^{(J-4)} + \mathcal{D}_{\beta u}^{(J+3)}$$

into irreducible representations of O_h should equal the decomposition of

$$\mathcal{D}_{1u}^{(J-1)} + \mathcal{D}_{1u}^{(J)},$$

which is impossible because no pair (α, β) can satisfy this additional restriction.

Further analysis of Fig. 5 shows that changing the sign of the Coriolis parameter k_3 not only alters the direction of the level transfer but also affects other aspects of cluster structure. Comparing top and bottom plots in Fig. 5 we can see that they differ in the position of clusters at the extremes of the branches. Normally we expect to find quantum levels inside the energy interval designated by the global maximum and minimum of the RES. This regular situation can be well seen near the C_4 maximum of the upper RES (Figs. 1, 2, and 5) where the oscillator like sequences of sixfold clusters begin one half of a quantum (one half the energy difference between the first two clusters in the sequence) below the classical limit energy. However, near other extremes of the two components the situation is different. Thus in the case $k_3 < 0$ (Fig. 5, bottom) an eightfold cluster of the central component is located right at the minimum classical energy corresponding to the rotation around the C_3 axis. The same component in the case $k_3 > 0$ (Fig. 5, top) does not have such cluster, and of course the sixfold cluster is moving along the classical C_4 energy curve when transferring between the components.

Finally, alternation of the sign of k_3 can be given a clear physical interpretation. The rotational part of the Coriolis term $H^{1(1_g,F_{1g})}$ is a rotational tensor of odd degree, namely $R_\alpha^{1(1_g,F_{1g})} = 2\hat{J}_\alpha$ with $\alpha = x, y, z$. Consequently, changing the sign of k_3 (and simultaneously of all parameters of the so-called "imaginary" terms $H^{\Omega(K_g,\Gamma)}$ with odd degree Ω of the rotational part) can be interpreted as changing the sign of the commutation relation between the angular momentum operators

$$[J_\alpha, J_\beta] = +\epsilon_{\alpha\beta\gamma} J_\gamma \rightarrow [J_\alpha, J_\beta] = -\epsilon_{\alpha\beta\gamma} J_\gamma,$$

Copyright © 2000 by Academic Press

with ϵ the totally antisymmetric tensor and α, β, γ standing for x, y, or z. The "+" relation holds in the laboratory fixed coordinate frame, whereas the "−" relation applies in the molecule-fixed frame. The same classical Hamiltonian matrix symbol can be associated with two quantum operators which differ in the signs of all odd Ω terms.

6. ASYMPTOTIC BEHAVIOR AND POSSIBLE HIGHER ORDER CONNECTION AT LARGE J

As we already mentioned above, our effective Hamiltonian is much less reliable at large values of J. Inclusion of higher order tensorial contributions to the effective Hamiltonian can seriously modify the qualitative structure of rotational bands in the $J > 60$ region where the number of experimental data is insufficient for the detailed reconstruction of the effective Hamiltonian. However it exhibits an interesting and rare behavior near $J = 70$, which we would like to mention. According to this Hamiltonian the two lowest RESs cross each other at the C_4 points when $J \simeq 71.36$. In contrast to the conical intersection at $J \approx 8$, this intersection is parabolic and corresponds to the step in the Hessian value computed at the corresponding C_4 points in the interval $J = 70 \cdots 75$ (Fig. 6).

Another interesting feature of the structure of the three components at high J is the near degeneracy of the C_4 minima of the two lower RES which lie much lower than the C_4 maximum of the upper RES. To explain this structure we can consider the limit of very high rotational excitation (large J) where the amplitude of the $\nu_6 = 1$ vibrations is small compared to the centrifugal distortion of the molecule. In this limit we consider vibrations about a J-dependent equilibrium configuration whose symmetry is generally lower than the O_h symmetry of the $J = 0$ equilibrium. This limit has been studied extensively in (*28, 29*).

Depending on the orientation of the rotation axis the distortion of the $J = 0$ equilibrium is different. Rotation around stationary axes C_4, C_3, and C_2 breaks the O_h symmetry of the equilibrium configuration down to D_{4h}, D_{3d}, and D_{2h}, respectively. Neither of these groups have, of course, triply degenerate irreducible representations, and therefore the triply degenerate vibrational mode $\nu_6(F_{1u})$ of the O_h symmetric molecule will split. Near the D_{4h} and D_{3d} equilibria the ν_6 mode splits into a nondegenerate and a doubly degenerate mode; near the D_{2h} equilibrium the ν_6 mode splits into a sum of three nondegenerate modes. This explains qualitatively why it is natural to expect that in the large J limit the two C_4 energies and the two C_3 energies become nearly degenerate while the three C_2 energies remain separated.

7. PURELY CLASSICAL ANALYSIS OF THE ROVIBRATIONAL HAMILTONIAN

So far our analysis was based on the classical limit of the rotational operators and on quantum three-state description of the vibrational problem. In this way we obtained three rotational energy surfaces (RESs) which represented three vibrational components. We can also introduce a completely classical limit where both rotation and vibration are treated classically. In this section we account briefly for the remarkable fact of the *exact* correspondence of the formulae [10], [11], and [12] obtained by the RES method and the results of the classical study of the relative equilibria (stationary points on the classical phase space defined by the critical orbits of the symmetry group) of the classical rotation–vibration Hamiltonian.

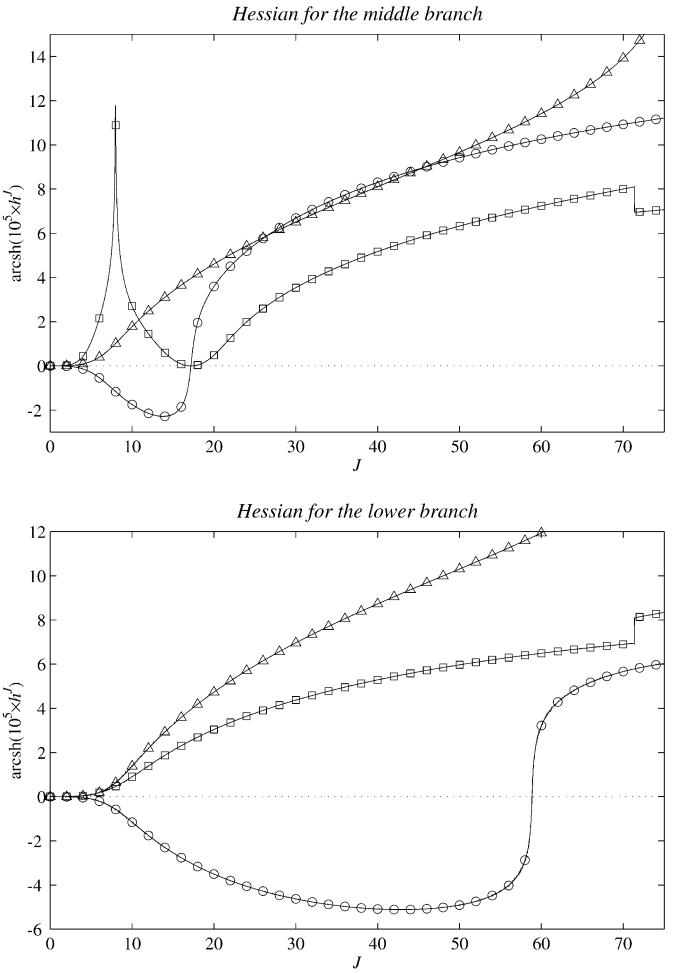

FIG. 6. Hessian values $\mathrm{arcsh}(10^5 \times h^J(\theta, \phi))$, at the stationary points of the central component $E_0(\mathcal{J})$ and lower component $E_+(\mathcal{J})$ of $\nu_6 = 1$ for J up to 75.

7.1. Classical Limit of the Vibrational Problem

To construct a purely classical analog of the quantum Hamiltonian [3] we should transform quantum operators of vibrational coordinates and conjugated momenta $(\hat{q}_i, \hat{p}_i)$, $i = 1, 2, 3$ of the triply degenerate oscillator to classical variables. To this end it suffices to replace $(\hat{q}_i, \hat{p}_i)$ for classical variables $(q_i,$

Copyright © 2000 by Academic Press

p_i). Equivalently, the classical analogs of the three creation and annihilation operators are the three complex variables together with their conjugates (*30*)

$$(a_k^+, a_k) \rightarrow (z_k^*, z_k) = (q_k + ip_k, q_k - ip_k), \quad k = 1, 2, 3.$$

A less trivial task is to understand the topology of the corresponding classical vibrational phase space. To do this we should realize that our problem contains an approximate integral of motion

$$\mathcal{N} = \frac{1}{2}(z_1 z_1^* + z_2 z_2^* + z_3 z_3^*) \qquad [32]$$

corresponding to the polyad quantum number n (total number of quanta in the ν_6 mode) of the quantum Hamiltonian. This integral is the harmonic oscillator part of the vibrational Hamiltonian or equally the sum of actions of the three one-dimensional oscillators. The assumption that n is preserved introduces an approximate dynamical symmetry. Reduction of this oscillator symmetry (see, for example Appendix B in (*31*)) leads from the initial six-dimensional Euclidean phase-space R_6 to a reduced-phase space of real dimension 4 which is a complex projective space CP_2. This space can be described in terms of homogeneous quadratic polynomials constructed of z and z^*; these polynomials are $su(3)$ analogs of the angular momenta J_x, J_y, J_z which describe the rotational sphere S_2. Analysis of the topological and group-theoretical features related with this model was initiated in (*9*) and continued later in (*12, 13*). Vibrational polyads of different kinds were intensively studied by Kellman (*32*). A numerical semiclassical analysis of the internal structure of vibrational polyads of a triply degenerate mode was suggested in (*33*).

7.2. Critical Orbits on the Classical Phase Space

Our classical analysis is very similar to the RES analysis of the purely rotational problem with classical phase-space S_2. We recall that in this latter familiar problem we look for stationary points of RES which in the presence of symmetry can be found, at least in the simplest possible situation, entirely from the action of the symmetry group on S_2. Thus in the case of cubic symmetry we find *isolated* points on S_2 which are fixed with regard to particular symmetry operations (rotation around particular axes C_4, C_3, and C_2). Operations which leave a particular point invariant form the local symmetry group of the point. This group is called a *stabilizer.* Other operations map the point to other points on S_2. All such points form an *orbit.* Since the points with local symmetry C_4, C_3, and C_2 are isolated, the corresponding orbits are *critical* (*23*). Any RES must have stationary points at the points in the critical orbits. In general, critical orbits correspond to *relative equilibria* of the problem, the set of equilibria of the reduced Hamiltonian which correspond to principal periodic orbits of the original problem (*29*). The values of the rotational Hamiltonian on the critical orbits or the energies of relative equilibria describe the cluster structure of the quantum multiplet.

The total classical phase space of our model rovibrational Hamiltonian for the $\nu_6(F_{1u})$ mode is the product $CP_2 \times S_2$ (for other examples of classical phase spaces of this kind see (*11, 17*)). Due to the action of the symmetry group O_h there are several critical orbits on this space. These critical orbits are necessarily stationary points of any smooth Morse function defined over $CP_2 \times S_2$. Critical orbits are defined entirely by the action of the O_h group on the vibrational and rotational spaces CP_2 and S_2, respectively. More precisely, since the spatial inversion does not modify angular momentum components and quadratic vibrational polynomials, the action of the O_h group reduces to that of the O group. (The image of O_h in the space of rotational and quadratic vibrational variables is O.) The action of the O group on CP_2 has been studied in detail in (*9*), and the action of this group on the rotational space S_2 [on (J_x, J_y, J_z)] is, of course, well known. The seven critical orbits of the O group action on the $CP_2 \times S_2$ space are characterized in Table 4, where for each orbit we specify its stabilizer on the total space, and on the vibrational and rotational subspaces CP_2 and S_2, the number of points in the orbit, and the branch assignment in the limiting case of normal Coriolis splitting. Positions of these critical orbits can be obtained directly from Table 4 of Ref. (*9*) and from the positions of critical orbits of the O group action on S_2. In Table 4 we give these positions in terms of complex vibrational coordinates z_k, $k = 1, 2, 3$ and rotational coordinates J_a, $a = x, y, z$. Since the energy (and everything else) is exactly the same for all points on the same critical orbit, only one point in each orbit is represented.

7.3. Other Stationary Points on $CP_2 \times S_2$

All points in the critical orbits in Table 4 are stationary points of any Morse function (a smooth function with only nondegenerate stationary points) defined on our phase space $CP_2 \times S_2$. However, using simple topology arguments we can show that such function should also have additional stationary points. We can also suggest that an O-symmetric Morse function on $CP_2 \times S_2$ would have two additional noncritical C_2 orbits of stationary points. Using the description of the O group action (*9*), we find that the points in question project on C_2-invariant spheres S_2 in CP_2. It is possible to characterize them further by taking the time reversal symmetry of our rovibrational Hamiltonian into account. Action of time reversal operation T on the classical variables

$$(z_1, z_2, z_3, J_x, J_y, J_z) \rightarrow (z_1^*, z_2^*, z_3^*, -J_x, -J_y, -J_z) \qquad [33]$$

is equivalent to simultaneous complex conjugation on CP_2 and inversion on S_2. Since the Hamiltonian itself is, of course,

Copyright © 2000 by Academic Press

TABLE 4
Critical Orbits of the Action of the O Group and Stationary Points of the Hamiltonian Function on the Classical Phase-Space $CP_2 \times S_2$

stabilizer of the orbit total	vib	rot	position on CP_2 (z_1, z_2, z_3)	position on S_2 (J_1, J_2, J_3)	type of orbit	number of points	component assignment
C_4	D_4	C_4	$\mathcal{N}(1,0,0)$	$\mathcal{J}(1,0,0)$	critical	6	central
C_4	C_4	C_4	$\frac{\mathcal{N}}{\sqrt{2}}(0,1,+i)$	$\mathcal{J}(1,0,0)$	critical	6	upper/lower
C_4	C_4	C_4	$\frac{\mathcal{N}}{\sqrt{2}}(0,1,-i)$	$\mathcal{J}(1,0,0)$	critical	6	lower/upper
C_3	D_3	C_3	$\frac{\mathcal{N}}{\sqrt{3}}(1,1,1)$	$\frac{\mathcal{J}}{\sqrt{3}}(1,1,1)$	critical	8	central
C_3	C_3	C_3	$\frac{\mathcal{N}}{2}\left(\frac{2}{\sqrt{3}}, -\frac{1}{\sqrt{3}} - i, -\frac{1}{\sqrt{3}} + i\right)$	$\frac{\mathcal{J}}{\sqrt{3}}(1,1,1)$	critical	8	upper/lower
C_3	C_3	C_3	$\frac{\mathcal{N}}{2}\left(\frac{2}{\sqrt{3}}, -\frac{1}{\sqrt{3}} + i, -\frac{1}{\sqrt{3}} - i\right)$	$\frac{\mathcal{J}}{\sqrt{3}}(1,1,1)$	critical	8	lower/upper
C_2	D_2	C_2	$\frac{\mathcal{N}}{\sqrt{2}}(0,1,1)$	$\frac{\mathcal{J}}{\sqrt{2}}(0,1,1)$	critical	12	central
$C_2 \wedge T_2$	$C_2 \wedge T_2$	$C_2 \wedge T_2$	$\frac{\mathcal{N}}{\sqrt{1+x^2}}\left(ix, \frac{1}{\sqrt{2}}, -\frac{1}{\sqrt{2}}\right)$	$\frac{\mathcal{J}}{\sqrt{2}}(0,1,1)$	non-critical	12	upper/lower
$C_2 \wedge T_2$	$C_2 \wedge T_2$	$C_2 \wedge T_2$	$\frac{\mathcal{N}}{\sqrt{1+y^2}}\left(iy, \frac{1}{\sqrt{2}}, -\frac{1}{\sqrt{2}}\right)$	$\frac{\mathcal{J}}{\sqrt{2}}(0,1,1)$	non-critical	12	lower/upper

Note. Reversing symmetry T_2 is used to restrict noncritical C_2 orbits to the corresponding invariant submanifold S_1 where the two orbits x and y represent the two stationary points of a generic Hamiltonian function.

invariant with respect to T, we can extend its initial symmetry group (*36*) from the spatial group O_h to $O_h \wedge T$ which on $CP_2 \times S_2$ becomes $O \wedge T$.

Analysis of the $O \wedge T$ action on $CP_2 \times S_2$ indicates the presence of a one-dimensional stratum formed by 12-point orbits whose stabilizer is the four-element group

$$C_2 \times T_2 = [Id,\ C_2',\ (C_4^2 \circ T),\ (C_2'' \circ T)].$$

(The C_2 subgroup of this group contains the C_2' element and the second-order-2 subgroup T_2 contains a reversing operation $T_2 = C_2'' \circ T$; the so-called "diagonal" axes C_2' and C_2'' are orthogonal to one of the C_4 axes.) This stratum is a union of 12 isolated S_1 circles. Each circle lies on the corresponding C_2-invariant sphere with stabilizer C_2'. A Morse function has two stationary points on S_1. These points are at the same time stationary on the C_2-invariant sphere in CP_2 and on the complete space $CP_2 \times S_2$ due to the $O \wedge T$ symmetry action. Of course, the exact position of the two stationary points depends on the concrete Hamiltonian function, but restricting this function to one of the invariant circles greatly facilitates the computation.

7.4. Energy of Relative Equilibria

Having done all preparatory analysis described above and having transformed our Hamiltonian [3] to its classical analogue $\mathcal{H}(z, J)$ we can appreciate the results. Indeed, we obtain the energies of all relative equilibria corresponding to critical orbits (in particular the energies of all C_4 and C_3 symmetric relative equilibria) after a trivial substitution of classical dynamical variables z and J in the Hamiltonian function $\mathcal{H}$ for the coordinates of the points in Table 4. If the scaling constant corresponding to the value of the oscillator integral $\mathcal{N}$ is set to 1, resulting analytic expressions are *identical* to those in Eqs. [10], [11], and [12] obtained from the analysis of the eigenvalues of the 3×3 matrix Hamiltonian [7] for the $\nu_6 = 1$ state.

To find explicitly the position of the two remaining C_2-symmetric stationary points and the energy of the corresponding relative equilibria, we restrict our classical Hamiltonian $\mathcal{H}$ to the S_1 subspace of CP_2 indicated in Table 4. The coordinates x and y of the two points are defined in terms of the polar coordinate ϕ on the circle S_1. They are obtained as solutions of a simple quadratic equation in ϕ defining the minimum and the maximum of $\mathcal{H}$ on S_1. Of course, positions x and y of the noncritical stationary points depend on the Hamiltonian parameters and the values of $\mathcal{J}$. As before, after replacing variables

Copyright © 2000 by Academic Press

z and J for the coordinates of the C_2 symmetric points in Table 4 and using the solutions for x and y (with $\mathcal{N} = 1$) we obtain expressions which can be transformed to form [12].

8. CONCLUSION

We once again demonstrated the advantages and usefulness of the simple classical approach to the analysis of rovibrational energy level system of concrete molecules. Using this approach we gave a complete concise qualitative description of the complicated rotational structure of the $\nu_6 = 1$ state of $Mo(CO)_6$.

We demonstrated how the global features of the rovibrational energy level patterns can be described and interpreted using simple classical mechanical models based on the concept of the rotational energy surface. Description of all stationary points and singularities in our classical model provides a way to understand and characterize all possible energy level structures, including energy intervals with regular sequences of states related to regular dynamical behavior and exceptional states and energy regions related to singularities. We do not, of course, characterize all individual quantum states, a nearly impossible task if our models are meant to be applicable at increasingly high energies where the number and density of states grow rapidly. The obvious advantage of the method is that the complexity of our calculations does not increase with the increase of the rotational excitation.

Our purely classical study (Section 7) based on $CP_2 \times S_2$ and the striking correspondence of its results to the RES calculations deserves by right further serious research which we plan for the near future. In general such classical study should be increasingly accurate in the analysis of the corresponding quantum system in the limit of high rotational *and* vibrational excitations. Nevertheless, our results indicate strongly that the analysis of classical relative equilibria on $CP_2 \times S_2$ can be very useful even in the study of low excited vibrational states which previously were always considered as exclusively quantum systems.

ACKNOWLEDGMENT

Région Bourgogne is gratefully acknowledged for supporting Laboratoire de Physique de l'Université de Bourgogne.

REFERENCES

1. A. J. Dorney and J. K. G. Watson, *J. Mol. Spectrosc.* **42,** 135–148 (1972).
2. W. G. Harter and C. W. Patterson, *J. Chem. Phys.* **66,** 4872–4885 (1977).
3. W. G. Harter, C. W. Patterson, and H. W. Galbraith, *J. Chem. Phys.* **69,** 4896–4907 (1978).
4. W. G. Harter and C. Patterson, *J. Chem. Phys.* **80,** 4241–4261 (1984).
5. I. Pavlichenkov and B. Zhilinskiĭ, *Chem. Phys.* **100,** 339 (1985); *Ann. Phys.* **184,** 1–32 (1988).
6. W. G. Harter, *Comp. Phys. Rep.* **8,** 319–394 (1988).
7. D. Sadovskiĭ and B. Zhilinskiĭ, *Mol. Phys.* **65,** 109–128 (1988).
8. V. Pavlov-Verevkin, D. Sadovskiĭ, and B. Zhilinskiĭ, *Europhys. Lett.* **6,** 573–578 (1988). [An entirely classical interpretation of the redistribution phenomenon and diabolic points is given in (*19*) where this phenomenon is associated with classical *monodromy*.]
9. B. Zhilinskiĭ, *Chem. Phys.* **137,** 1–13 (1989).
10. V. Krivtsun, D. Sadovskiĭ, and B. Zhilinskiĭ, *J. Mol. Spectrosc.* **139,** 126–146 (1990).
11. D. Sadovskiĭ and B. Zhilinskiĭ, *Phys. Rev. A: Gen. Phys.* **47,** 2653–2671 (1993).
12. D. Sadovskiĭ and B. Zhilinskiĭ, *Phys. Rev. A: Gen. Phys.* **48,** 1035–1044 (1993).
13. N. Fulton, J. Tennyson, D. A. Sadovskiĭ, and B. I. Zhilinskiĭ, *J. Chem. Phys.* **99,** 906–918 (1993).
14. B. Zhilinskiĭ and S. Brodersen, *J. Mol. Spectrosc.* **163,** 326–338 (1994).
15. S. Brodersen and B. Zhilinskiĭ, *J. Mol. Spectrosc.* **172,** 303–318 (1995).
16. S. Brodersen and B. Zhilinskiĭ, *J. Mol. Spectrosc.* **169,** 1–17 (1995).
17. B. Zhilinskiĭ, *Spectrochim. Acta A* **52,** 881–900 (1996).
18. L. Michel and B. Zhilinskiĭ, Technical Report No. IHES/P/97/54, Institut des Hautes Etudes Scientifiques Bures-sur-Yvette (France) (unpublished).
19. D. A. Sadovskiĭ and B. Zhilinskiĭ, *Phys. Lett. A* **256,** 235–244 (1999).
20. P. Asselin, P. Soulard, L. Manceron, V. Boudon, and G. Pierre, *J. Mol. Struct.,* in press.
21. L. Jones, R. McDowell, and M. Goldblatt, *Inorg. Chem.* **8,** 2340–2363 (1969).
22. J.-P. Champion, M. Loëte, and G. Pierre, *in* "Spectroscopy of the Earth's Atmosphere and Interstellar Medium," (K. N. Rao and A. Weber, Eds.), Academic Press, San Diego, 1992, pp. 339–422.
23. L. Michel, *Rev. Mod. Phys.* **52,** 617–651 (1980).
24. A. Robiette, D. Gray, and F. Birss, *Mol. Phys.* **32,** 1591–1607 (1976).
25. G. Herzberg, "Molecular Spectra and Structure. II. Infrared and Raman Spectra of Polyatomic Molecules," Van Nostrand, New York, 1966.
26. I. M. Pavlichenkov, *Phys. Rep.* **226,** 173–279 (1993).
27. G. Pierre, D. Sadovskiĭ, and B. Zhilinskiĭ, *Europhys. Lett.* **10,** 409–414 (1989).
28. I. Kozin, R. M. Roberts, and J. Tennyson, *J. Chem. Phys.* **111,** 140–150 (1999).
29. J. Montaldi and R. M. Roberts, *J. Nonlinear Sci.* **9,** 53–88 (1999).
30. V. Bargmann, *Comm. Pure Appl. Math.* **14,** 187–214 (1961).
31. R. Cushman and L. M. Bates, "Global Aspects of Classical Integrable Systems," Birkhauser, Basel, 1997.
32. M. Kellman, *in* "Molecular Dynamics and Spectroscopy by Stimulated Emission Pumping," (H.-L. Day and R. Field, Eds.), World Scientific, Singapore, 1995, pp. 1–60.
33. C. Patterson, *J. Chem. Phys.* **83,** 4618–4632 (1985).
34. D. A. Sadovskiĭ, B. I. Zhilinskiĭ, and L. Michel, *Phys. Rev. A: Gen. Phys.* **53,** 4064–4067 (1996).
35. D. A. Sadovskiĭ and B. I. Zhilinskiĭ, *Phys. Rev. A: Gen. Phys.* **57,** 2867–2884 (1998).
36. [Similar extension of a spatial symmetry group by reversing operations has turned out to be extremely useful in the qualitative analysis of many problems, such as the simple model three-level Hamiltonian with $SU(3)$ dynamical symmetry (*12*) and the Hamiltonian of the hydrogen atom in the presence of external electric and magnetic fields (*18, 34, 35*).]

Copyright © 2000 by Academic Press